

Monte Carlo Studies of Geomagnetic Field Effects on the Imaging Air Cherenkov Technique for the MAGIC Telescope Site

S.C. Commichau ^{a,*}, A. Biland ^a, J.L. Contreras ^b,
R. de los Reyes ^b, A. Moralejo ^c, J. Sitarek ^{d,e}, D. Sobczyńska ^e
on behalf of the MAGIC collaboration ¹

^a*ETH Zurich, CH-8093 Switzerland*

^b*Universidad Complutense, E-28040 Madrid, Spain*

^c*Institut de Física d'Altes Energies, Edifici Cn., E-08193 Bellaterra (Barcelona), Spain*

^d*Max-Planck-Institut für Physik, D-80805 München, Germany*

^e*University of Łódź, PL-90236 Lodz, Poland*

Abstract

Imaging air Cherenkov telescopes (IACTs) detect the Cherenkov light from extensive air showers (EAS) initiated by very high energy (VHE) γ -rays impinging on the Earth's atmosphere. Due to the overwhelming background from hadron induced EAS, the discrimination of the rare γ -like events is vital. The influence of the geomagnetic field (GF) on the development of EAS can further complicate the imaging air Cherenkov technique. The amount and the angular distribution of Cherenkov light from EAS can be obtained by means of Monte Carlo (MC) simulations. Here we present the results from dedicated MC studies of GF effects on images from γ -ray initiated EAS for the MAGIC telescope site, where the GF strength is $\sim 40 \mu\text{T}$. The results from the MC studies suggest that GF effects degrade not only measurements of very low energy γ -rays below $\sim 100 \text{ GeV}$ but also those at TeV-energies.

Key words: Extensive air showers, Monte Carlo simulations, gamma-ray, Geomagnetism

PACS: 96.50.sd, 87.10.Rt, 95.85.Pw, 91.25.-r

* Corresponding author. Tel.: +41-44-63 32185; fax.: +41-44-63 31104

Email address: sebastian.commichau@phys.ethz.ch (S.C. Commichau).

¹ *URL:* <http://wwwmagic.mppmu.mpg.de/collaboration/members/index.html>

1 Introduction

Imaging air Cherenkov telescopes (IACTs) aim at the detection of Cherenkov light from extensive air showers (EAS) initiated by very high energy (VHE) γ -rays impinging on the Earth's atmosphere. IACTs make use of the differences between the angular distributions of Cherenkov light from γ -ray and hadron induced EAS to efficiently discriminate the hadronic background. Due to the overwhelming abundance of hadrons in the cosmic rays (mostly protons), the discrimination of the rare γ -ray events is rather difficult, in particular for energies below 100 GeV. Only a small fraction of the recorded data are due to γ -ray initiated EAS. The influence of the geomagnetic field (GF) on the development of EAS can further complicate the suppression of the hadronic background and therefore reduces the sensitivity of an instrument. In addition, GF effects can systematically affect the energy resolution of an IACT [1,2,3].

The influence of the GF on EAS was already qualitatively discussed in 1953 [4]. It was pointed out that the east-west separation of electrons and positrons in EAS due to the GF can be non-negligible compared to the displacement from multiple Coulomb scattering. Furthermore, the Lorentz force systematically deflects the particles into opposite directions whereas the displacement due to multiple Coulomb scattering is random. It was also argued that GF effects are relatively less important for hadron induced EAS than for γ -ray induced EAS. The scattering angles occurring in nuclear interactions of hadronic EAS give rise to a lateral displacement of the shower particles much larger than that due to the influence of the GF. The comparatively large transverse momenta of the secondary particles result in a large angular spread of the directions of the electromagnetic sub-cascades generated by pion decay.

The influence of the GF on the average lateral spread of atmospheric Cherenkov radiation was studied by means of computer simulations already more than 30 years ago [5]. GF effects on real γ -ray and proton initiated EAS were later on studied using a non-imaging Cherenkov telescope [6]. It was reported that the influence of the GF on proton initiated EAS results in a significant reduction of the count rate. It was shown elsewhere [7] that IACT measurements of TeV γ -rays from the Crab nebula were not significantly affected when the component of the GF normal to the shower axis, i.e. transversal component of the GF, was below $35 \mu\text{T}$. The average shape and reconstructed intensity of Cherenkov images from hadrons was found to be independent of the transversal component of the GF. However, it was pointed out that the instrument was not sensitive enough to study GF effects. More recent measurements of γ -ray showers carried out with a transversal component of the GF strength of $|\vec{B}_\perp| > 40 \mu\text{T}$ revealed GF effects in observational data compatible to those predicted by MC simulations, both for γ -ray and hadron showers [8,9]. The authors suggest that for EAS developing under unfavourable orientation with respect to the direction of the GF the corresponding Cherenkov light images

in the camera of an IACT will be rotated. As the information on the orientation of shower images provides the most powerful discrimination between γ -ray shower images from a point-like source and any unwanted isotropic background (mainly due to hadrons) this results in a degradation of the sensitivity of an IACT. However, it was demonstrated that a correction for GF effects in γ -ray initiated Cherenkov images is possibly resulting in an increased detection significance and better sensitivity of the IACT [10,11]. The correction for GF effects required simulated γ -ray showers.

IACTs currently in operation offer improved imaging capabilities, i.e. better optical point spread function (PSF), pixel resolution and timing capabilities of the electronics, and are therefore more sensitive to GF effects than previous instruments.

In this paper we present results from dedicated MC studies of GF effects on the imaging technique. The studies were carried out for the Major Atmospheric Gamma-ray Imaging Cherenkov (MAGIC) telescope [12,13], which is located on the Canary Island of La Palma at the Roque de los Muchachos Observatory at 2200 m altitude (28.45° N, 17.54° W).

2 The MAGIC Telescope

The 17 m diameter MAGIC telescope is currently the largest single dish IACT in operation. The imaging camera in the focal plane of the tessellated parabolic reflector consists of 577 photomultiplier tubes (PMTs), all of which are arranged in a hexagonal configuration. The inner part of the camera is equipped with 397 PMTs of a diameter of 0.1° whereas the outer part is equipped with larger PMTs of a diameter of 0.2° . The reflector has a focal length of 17 m. The field of view of the camera is 3.5° and the angular resolution for γ -rays is about 0.1° , depending on the energy. The telescope is in continuous operation since summer 2004. It allows for a detection of a γ -ray source with an absolute intensity of $\sim 2\%$ of the Crab nebula and similar energy spectrum within 50 hours at energies > 200 GeV on a significance level of 5 standard deviations.

MAGIC is currently being upgraded through the addition of a twin telescope to achieve an improved sensitivity and a lower energy threshold [14]. Further technical details and information on the performance of the instrument can be found elsewhere [15].

3 The Geomagnetic Field at the MAGIC Site

The component of the GF normal to the shower axis is relevant for the east-west separation of electrons and positrons during the shower development. For this study the telescope optical axis has always been set parallel to the direction of the primary γ -ray.

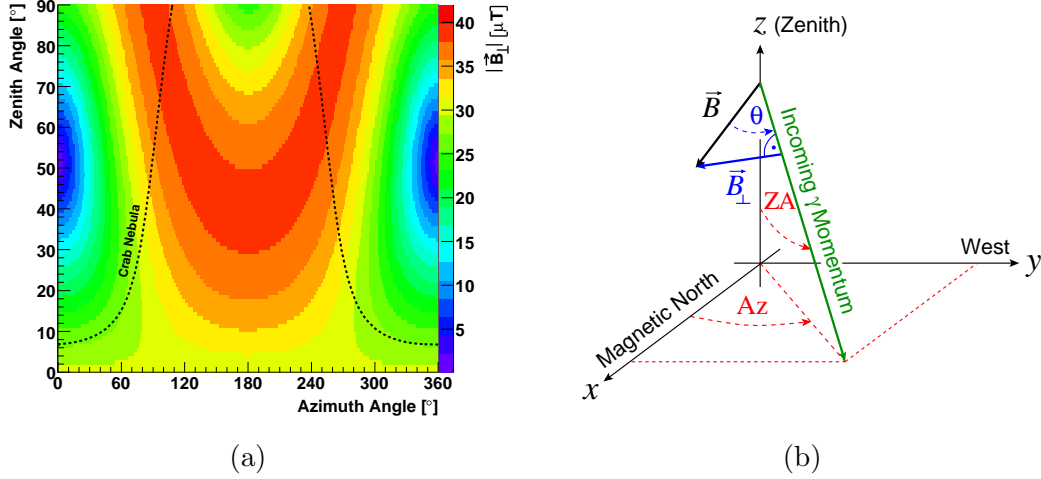


Fig. 1. (a) The absolute value of the component of the GF normal to the direction of the EAS versus azimuth (Az) angle and zenith angle (ZA) for the Roque de los Muchachos observatory on La Palma. (b) The definition of the coordinate system used throughout this work. θ denotes the angle between the direction of the EAS and the direction of the GF. The Az angle is defined like in the CORSIKA program [16], i.e. it refers to the momentum of the incoming γ -ray and is counted counterclockwise from the positive x -axis towards west. The telescope optical axis has always been set parallel to the direction of the primary γ -ray.

Figure 1 (a) shows the absolute value of the GF component $|\vec{B}_\perp|$ normal to the direction of the EAS versus azimuth (Az) angle and zenith angle (ZA) for the MAGIC telescope site. The value was determined for 10 km a.s.l. according to the epoch 2005 International Geomagnetic Reference Field (IGRF) model [17]. The MAGIC telescope is focused to a distance of 10 km a.s.l., which is the most likely location of the shower maximum for 100 GeV γ -ray induced EAS at small ZAs. The trajectory of the strongest source of steady VHE γ -ray emission in the Galaxy, the Crab nebula, is indicated. As the magnetic field lines at La Palma are tilted by $\sim 7^\circ$ westwards with respect to the meridian [17] the trajectory is asymmetric with respect to 180° Az angle. For La Palma, the minimum influence of the GF is expected to occur for EAS developing in direction of the magnetic north at $ZA = (90^\circ - I) \approx 51^\circ$ and $Az = 0^\circ$, where the angle θ between the shower axis and the GF becomes smallest (see figure 1 (b)), i.e. for EAS developing along the field lines. I denotes the angle under which the GF lines dip into the Earth's surface, which

is $\sim 39^\circ$ for La Palma [17]. Hence, the maximum influence is expected for EAS developing perpendicular to the direction of the GF lines, i.e. for $ZA \approx 39^\circ$ and $Az = 180^\circ$.

The results from the MC studies on the GF effects presented here are specific to the MAGIC telescope because of the local GF strength and the relevant telescope parameters like the reflector area, camera pixelisation and the γ -ray PSF.

4 Monte Carlo Simulations

The production of Monte Carlo (MC) data for MAGIC involves three steps [18]:

1. The CORSIKA (COsmic Ray SIMulations for KAscade) MC program (version 6.019) [16] is used to simulate the development of γ -ray and hadron induced extensive air showers (EAS) and the production of Cherenkov light for a given set of input parameters, like the primary γ -ray or hadron energy, height above sea level, the magnitude and direction of the GF, and so on. The GF components are set to the values for the location of the MAGIC telescope (La Palma, 28.8° N, 17.9° W) which are provided by the IGRF model [17]. The x -axis of the Cartesian CORSIKA reference frame is aligned with the magnetic north pole and the y -axis points to the west. The Az angle is counted counterclockwise from the positive x -axis and refers to the direction of the primary γ -ray (figure 1 (b)). Furthermore, the so-called US standard atmosphere is used as a model for the Earth's atmosphere.
2. The binary output of CORSIKA, containing information on the Cherenkov photon direction and its position on ground, is processed with a dedicated *Reflector* program, which does the ray-tracing of the Cherenkov photons. To be able to adapt to different conditions without being forced to rerun CORSIKA, atmospheric absorption and scattering of Cherenkov photons as well as mirror condition is taken into account at this stage.
3. Finally, the output of the *Reflector* program is processed by the *Camera* program simulating the entire readout chain, i.e. PMT response, trigger and data acquisition system including electronic noise. Normally, a compact next-neighbour coincidence is required, i.e. at least four neighbouring pixels are required to trigger, and, if any of the pixels is taken out of the group, the remaining pixels are still neighbours. To adapt the MC data to the optical performance of the telescope, the simulation of the optical point spread function (PSF) can be tuned at this stage. The calibration and the image parameter calculation (Hillas analysis [19]) is done using the MAGIC Analysis and Reconstruction Software (MARS) [20].

137 For the present studies only γ -rays were simulated. The MC data were pro-
 138 duced following for most instances the standard MC production of the MAGIC
 139 telescope as described beforehand. All events were simulated as originating
 140 from a point source. By definition, the telescope optical axis is always parallel
 141 to the direction of the primary γ -ray. The impact parameter (IP) is defined as
 142 the distance from the centre of the telescope mirror to the shower axis, which
 143 has the same direction as the primary γ -ray.

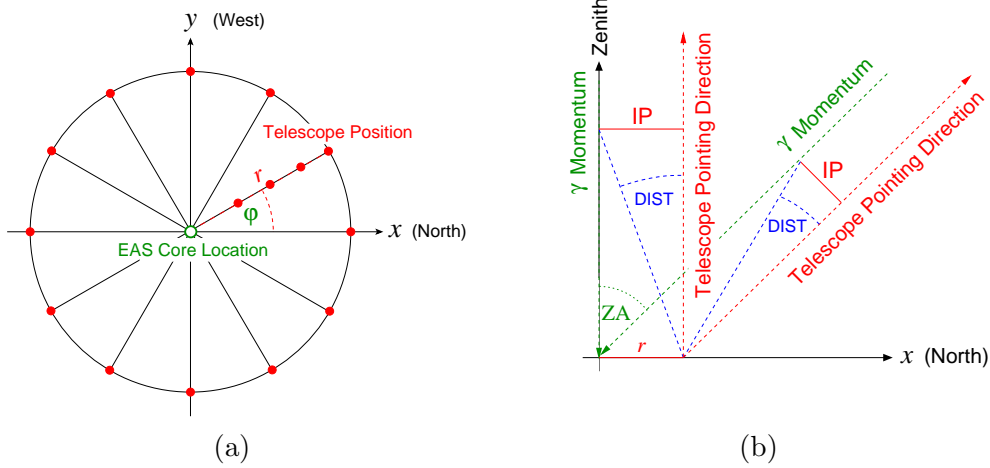


Fig. 2. (a) An illustration of the setup used in the MC simulations: the telescope positions are indicated as full circles and the EAS core location (the primary γ -ray impact point on the ground) as an open circle. The impact distance on ground r is defined as the distance between the EAS core location and the telescope position. The telescope is situated always somewhere in the circle within which Cherenkov photons are kept. The simulations were done for fixed impact distances on ground $r = 20\text{ m}, \dots 180\text{ m}$ and angles $\varphi = 0^\circ, 30^\circ, \dots 330^\circ$. (b) The relation between the impact parameter (IP) and the impact distance r on the ground is illustrated. In direction of the telescope's inclination the impact parameter equals $r \cos(ZA)$.

144 In contrast to the production of standard MC data, where the EAS core loca-
 145 tion is randomly placed somewhere in a circle on the plane perpendicular to the
 146 direction of the EAS (to estimate the telescope effective collection area), the
 147 EAS for this study were simulated for fixed core locations and all Cherenkov
 148 photons arriving in a circle of 200 m radius were kept. This procedure reduces
 149 computing time because each CORSIKA event can be used multiple times by
 150 placing the telescope (at the level of the *Reflector* program) somewhere into
 151 the circle within which Cherenkov photons are kept (figure 2 (a)). Besides,
 152 this approach allows to study the influence of the GF on the shower images
 153 in great detail. For technical reasons the telescope was placed on equidistant
 154 points concentrically to the EAS core location. By the choice of this setup,
 155 the impact parameter varies like $r\sqrt{\cos^2(Az - \varphi)(\cos^2(ZA) - 1) + 1}$ (figure 2

(b)), where r is the distance between the EAS core location and the telescope position.

The energy of the primary γ -ray was for different samples set to 30 GeV, 50 GeV, 70 GeV, 120 GeV, 170 GeV, 300 GeV, 450 GeV or 1 TeV, respectively. The ZA was varied between 0° and 60° in steps of 20° , and the Az angle between 0° and 180° in steps of 30° , as the absolute value of the GF component normal to the EAS direction is symmetric in the Az angle (figure 1 (a)). Hence, the maximum value for the angle θ achieved with the simulated telescope orientations is 87° . The choice of discrete values for the γ -ray energy allows to investigate the energy dispersion of the showers due to the GF. The distance r between the telescope position and the EAS core location (impact point of the primary γ -ray on the ground) was varied between 20 m and 180 m in steps of 20 m and the angle φ (figure 2 (a)) between 0° and 330° in steps of 30° , resulting in 108 configurations.

About 10^5 events were simulated for each γ -ray energy, ZA and Az angle. As a reference, MC data were also produced without GF. To be as realistic as possible the MC simulations include the effects of photons from the diffuse night sky background of $1.75 \cdot 10^{12} \text{ ph m}^{-2} \text{ s}^{-1} \text{ sr}^{-1}$ at the MAGIC site [21] as well as electronic noise.

5 Image Analysis

The MC-generated γ -ray showers were analysed using the standard MAGIC software MARS [20]. Before parameterisation of the shower images a tail-cut image cleaning was applied (figure 3 (a)) [15]. The image cleaning requires the signals to be above a certain level. For the MC studies presented here the minimum required pixel content was 7 photoelectrons (phe) for so-called core pixels and 4 phe for boundary pixels.

Shower images from γ -ray showers processed with the image cleaning are narrow and point towards the source position in the field of view. To a first approximation the shower images are elliptical and can be described by so-called Hillas parameters [19]. Detailed reviews on the imaging technique can be found elsewhere [7,22]. Some of the image parameters used for these studies are illustrated in figure 3 (b). The parameters WIDTH and LENGTH characterise the lateral and longitudinal spread of the shower images (minor and major axes of the so-called Hillas ellipse). Both parameters are very important since they allow a powerful discrimination of γ -ray images against hadron induced images. The parameters DIST and ALPHA are related to the position and orientation of shower images in the camera. The parameter DIST is directly related to the impact parameter of the primary γ -ray (figure 2 (b)). The image parameter ALPHA is commonly used by standalone IACTs to extract the γ -ray signal. ALPHA denotes the angle between the major axis of the

196 shower image and the vector connecting its centre of gravity with the source
 197 position in the camera plane (camera centre). It provides a very powerful dis-
 198 crimination between γ -ray images from a point-like source and any isotropic
 199 background (mainly due to hadrons), i.e. orientation discrimination. The γ -
 200 ray signal from a VHE γ -ray source under study appears as an excess at small
 201 values in the ALPHA parameter distribution.

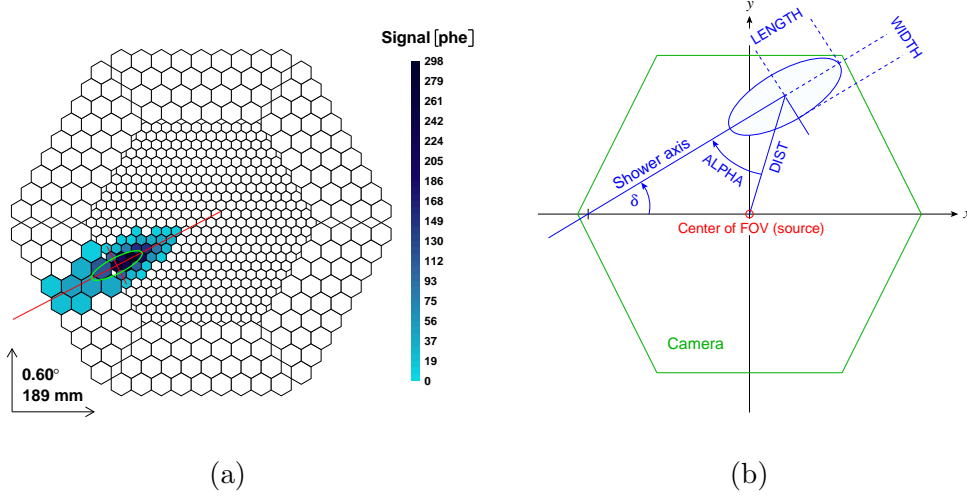


Fig. 3. (a) A MC-generated γ -ray shower image after application of the image cleaning. Only pixels surviving the image cleaning are used for the following steps of the analysis. (b) Definition of the image parameters. The light distribution is described by an ellipse whose major and minor axes describe the longitudinal and lateral spread of the Cherenkov light distribution.

202 Another viable image parameter is the so-called SIZE, which corresponds to
 203 the total integrated light of a shower image after treatment with the image
 204 cleaning procedure. It is therefore an estimate for the primary γ -ray energy.
 205 The so-called DISP method [23,24] allows to reconstruct the arrival direction
 206 of γ -ray candidates making use of the shape of a shower image. The DISP
 207 parameter is determined according to the formula

$$\text{DISP} = c_1(\text{SIZE}) + c_2(\text{SIZE}) \cdot \frac{\text{WIDTH}}{\text{LENGTH}}. \quad (1)$$

208 Therein c_1 and c_2 are second-order polynomials optimised on MC simulated
 209 γ -ray showers [25]:

$$c_1 = +1.163^\circ + 0.542^\circ (\log_{10}(\text{SIZE}) - 2) - 0.672^\circ (\log_{10}(\text{SIZE}) - 2)^2,$$

$$c_2 = -0.265^\circ - 2.905^\circ (\log_{10}(\text{SIZE}) - 2) + 2.220^\circ (\log_{10}(\text{SIZE}) - 2)^2.$$

210 In case of a single telescope the DISP method provides two possible solutions
 211 for the source position. To overcome this ambiguity the asymmetry of the

212 shower image along the major image axis, which is related to the longitudinal
 213 development of an EAS in the atmosphere, is used to reconstruct the true
 214 source position. However, owing to false head-tail assignment the percentage
 215 of correctly reconstructed events is typically limited to $\sim 80\%$, depending on
 216 the γ -ray energy [25]. The outcome of the DISP analysis is usually displayed
 217 in terms of a sky map of arrival directions. Because the DISP parameter
 218 depends on both the eccentricity WIDTH/LENGTH and on the orientation
 219 of the shower images the influence of the GF on the shower development is
 220 expected to degrade also the DISP method.
 221 In this paper, we restrict ourselves to selected but representative results from
 222 the MC study.

223 6 Results and Discussion

224 6.1 GF Effects on Shape and Orientation of γ -ray Shower Images

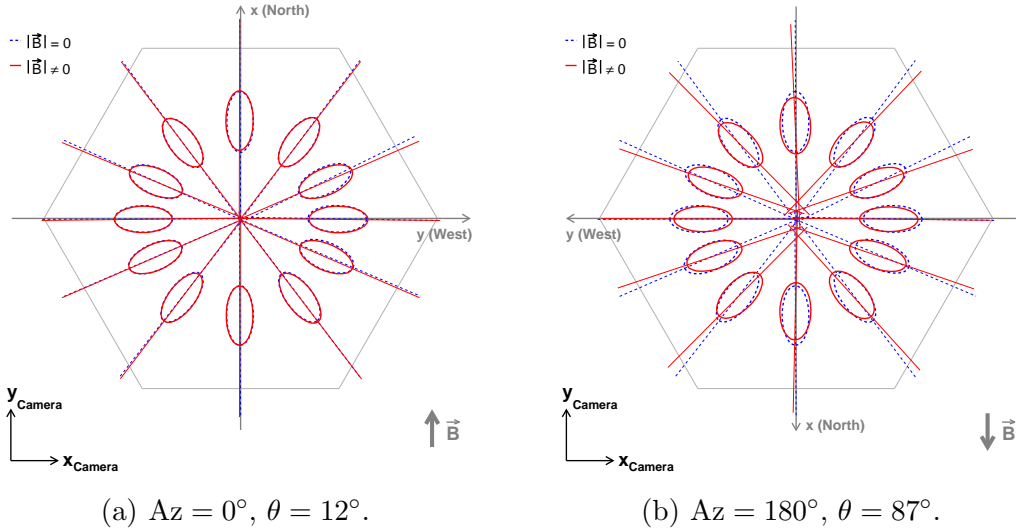
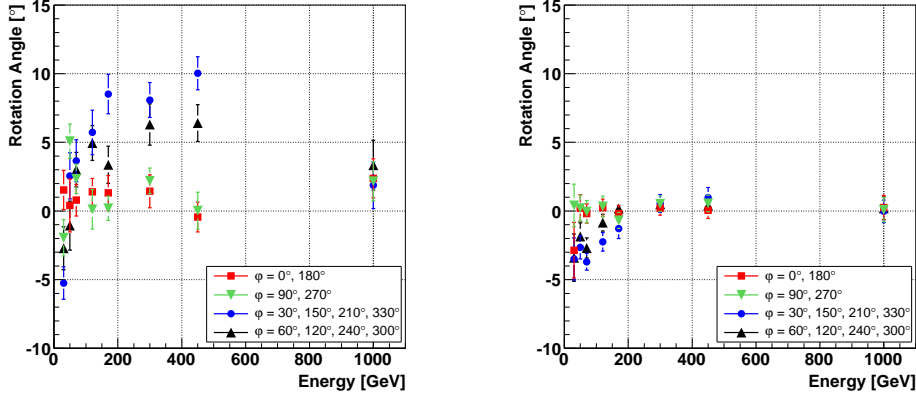


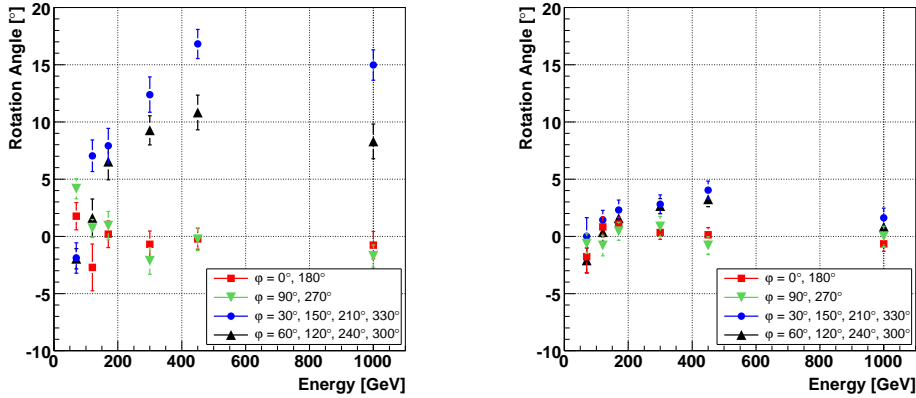
Fig. 4. Shower images in the telescope camera for 450 GeV γ -rays, 100 m impact parameter, $ZA = 40^\circ$, $Az = 0^\circ$ and 180° , respectively. The images indicated by solid lines were obtained for enabled GF and the ones indicated by dashed lines were obtained for disabled GF. The orientation of the GF component normal to the direction of the EAS (telescope pointing direction) is indicated in the lower right part of the figures (see text for more details).

225 The orientation of the γ -ray images from a source under study is used for the
 226 suppression of the isotropic hadronic background. It is accordingly important
 227 to study how the GF influences the orientation of shower images. Figure 4
 228 shows shower images (Hillas ellipses) in the telescope camera for 450 GeV γ -
 229 rays, 100 m impact parameter, $ZA = 40^\circ$, and different Az angles between 0°

230 and 180° . The ellipses drawn with solid lines were obtained for enabled GF
 231 and the ones drawn with dashed lines for disabled GF in the MC simulation.
 232 For each angle $\varphi = 0^\circ, 30^\circ, \dots, 330^\circ$ the size, the position and the orientation of
 233 the ellipse in the camera was determined by taking the mean values from the
 234 corresponding Hillas parameter distribution. The ellipses are superimposed
 235 on the projection of the CORSIKA coordinate system, whose x -axis is aligned
 236 with the magnetic north. The direction of the GF component normal to the
 237 direction of the EAS is indicated in the lower right part of the figures.

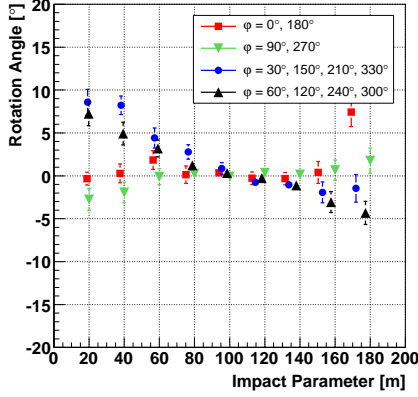


(a) $Az = 0^\circ$, $ZA = 0^\circ$, $IP = 40$ m, $\theta = 52^\circ$.
 (b) $Az = 0^\circ$, $ZA = 0^\circ$, $IP = 120$ m, $\theta = 52^\circ$.

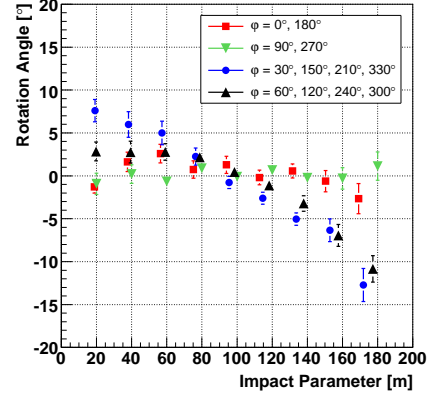


(c) $Az = 180^\circ$, $ZA = 40^\circ$, $IP \approx 40$ m, $\theta = 87^\circ$.
 (d) $Az = 180^\circ$, $ZA = 40^\circ$, $IP \approx 120$ m, $\theta = 87^\circ$.

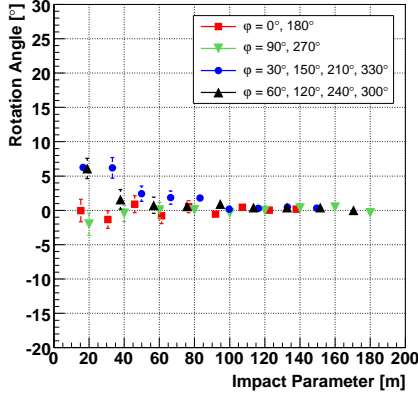
Fig. 5. The rotation angle of γ -ray images versus energy for 40 m and 120 m impact parameter, $ZA = 0^\circ, 40^\circ$, $Az = 0^\circ$ and 180° . Full triangle down data points correspond to the case where the connecting line between the EAS core location on ground and the telescope position is parallel to the north-south direction (x -axis), while for full square data points the telescope is situated on the y -axis. Full triangle up and full circle data points correspond to intermediate telescope positions.



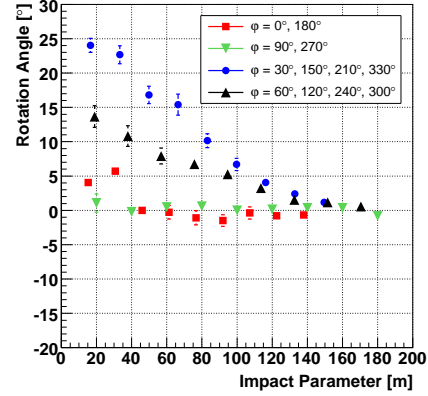
(a) $Az = 0^\circ$, $ZA = 20^\circ$, 120 GeV energy, $\theta = 32^\circ$.



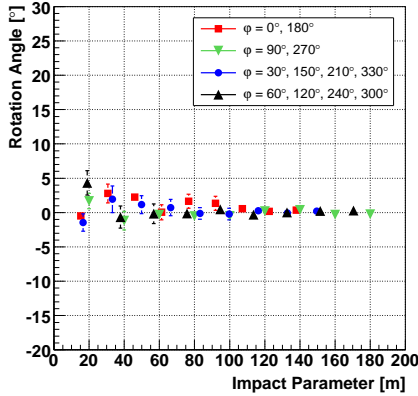
(b) $Az = 180^\circ$, $ZA = 20^\circ$, 120 GeV energy, $\theta = 72^\circ$.



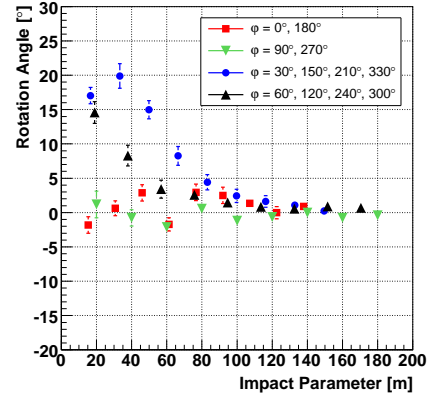
(c) $Az = 0^\circ$, $ZA = 40^\circ$, 450 GeV energy, $\theta = 12^\circ$.



(d) $Az = 180^\circ$, $ZA = 40^\circ$, 450 GeV energy, $\theta = 87^\circ$.

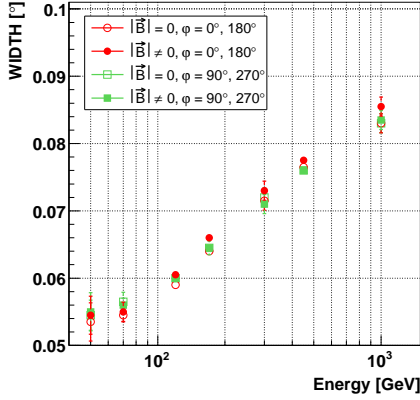


(e) $Az = 0^\circ$, $ZA = 40^\circ$, 1 TeV energy, $\theta = 12^\circ$.

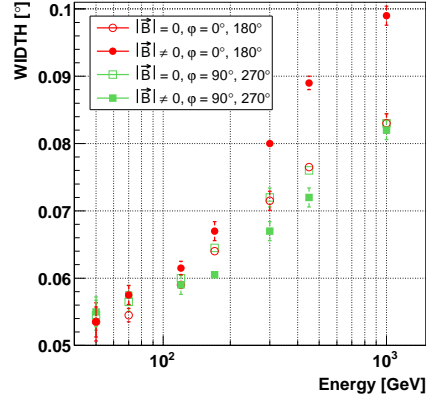


(f) $Az = 180^\circ$, $ZA = 40^\circ$, 1 TeV energy, $\theta = 87^\circ$.

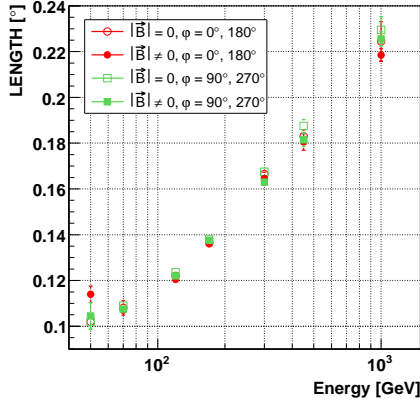
Fig. 6. The rotation angle of γ -ray images versus impact parameter for $ZA = 20^\circ$ and 40° , $Az = 0^\circ$ and 180° , 120 GeV, 450 GeV and 1 TeV energy (see text for more details).



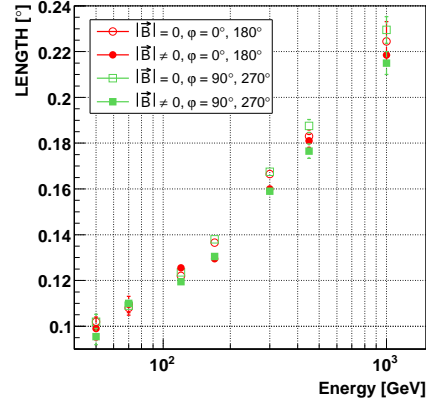
(a) $Az = 0^\circ, \theta = 12^\circ$.



(b) $Az = 180^\circ, \theta = 87^\circ$.



(c) $Az = 0^\circ, \theta = 12^\circ$.



(d) $Az = 180^\circ, \theta = 87^\circ$.

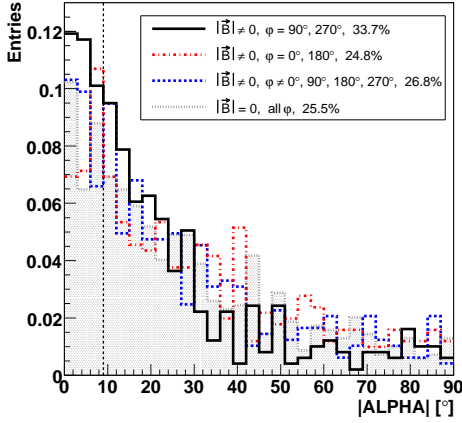
Fig. 7. The average WIDTH and LENGTH of γ -ray images versus energy for 120 m impact parameter, $ZA = 40^\circ$, $Az = 0^\circ$ and 180° (see text for more details).

As can be seen the average orientation is preserved only for shower images oriented either parallel or normal to the projected direction of the GF in the camera, which is by definition the GF component normal to the direction of the EAS (telescope pointing direction). Shower images situated at intermediate angles are systematically rotated away from the projected direction of the GF. The sideways spread of the images result in a systematic rotation away from the camera centre (source position). This was also reported in [10]. The magnitude of the rotation depends not only on the angle θ between the axis of the EAS and the direction of the GF but mainly on the core position of the EAS with respect to the telescope, which is given by the angle φ . By comparing the orientations for images generated with disabled GF to the ones for enabled GF it is possible to determine the rotation angle. Figure 5 shows the rotation angle of γ -ray images versus energy for an impact parameter of 40 m and 120 m. The figures show that the rotation angle depends on the impact parameter and on the γ -ray energy. However, the average rotation

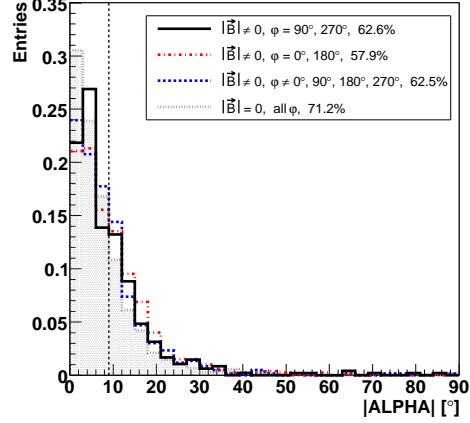
253 angle for images oriented either parallel or normal to the direction of the GF in
 254 the camera is zero (full square and full triangle down data points). Images ori-
 255 ented at intermediate angles are systematically rotated. For $ZA = 0^\circ$, $Az = 0^\circ$
 256 and 40 m impact parameter (figure 5 (a)) and for $ZA = 40^\circ$, $Az = 180^\circ$ (figure
 257 5 (c) and (d)), which is the most unfavourable telescope pointing direction,
 258 the rotation angle is maximal for γ -ray energies around 450 GeV.
 259 Figure 6 illustrates the dependency of the rotation angle on the impact pa-
 260 rameter. Small impact parameters correspond to images with low eccentricity
 261 WIDTH/LENGTH, which may be rotated through a large angle. Figure 6 (b)
 262 also shows that the direction of the rotation depends on the impact parame-
 263 ter. The shower images are not always rotated away from the direction of the
 264 GF in the camera but can even be rotated towards it. Consequently, the cor-
 265 rection of observational data for GF effects by de-rotating the shower images
 266 must take into account the energy dependence of the rotation angle and its
 267 dependence on the impact parameter (DIST). For the most unfavourable tele-
 268 scope pointing direction and for small impact parameters even 1 TeV shower
 269 images are rotated through a large angle (figure 6 (f)). The influence of the
 270 GF on the shape of the γ -ray shower images also depends on the primary
 271 γ -ray energy, the impact parameter and the orientation of the EAS relative to
 272 the direction of the GF. Figure 7 shows the average WIDTH and LENGTH
 273 of γ -ray images versus energy for 120 m impact parameter, $ZA = 40^\circ$, and 0°
 274 as well as $Az = 180^\circ$. For the most unfavourable telescope pointing direction,
 275 i.e. $ZA = 40^\circ$ and $Az = 180^\circ$ ($\theta = 87^\circ$) significant GF effects on the image pa-
 276 rameter WIDTH occur for γ -ray energies above ~ 100 GeV (figure 7 (b)). The
 277 influence of the GF on the image parameter WIDTH is considerably larger
 278 than on LENGTH. Due to the influence of the GF the average WIDTH is
 279 increased for images where the connecting line between the EAS core location
 280 on ground and the telescope position is parallel to the magnetic north-south
 281 direction (telescope situated on the x -axis, full and open circle data points).
 282 Images aligned with the direction of the GF in the camera are horizontally
 283 stretched compared to the situation of disabled GF in the MC, whereas im-
 284 ages oriented normal to the direction of the GF have a smaller WIDTH and
 285 are thus elongated due to the influence of the GF (telescope situated on the
 286 y -axis, full and open square data points).

287 6.2 GF Effects on the Image Parameter ALPHA

288 In the preceding section it was shown that the GF can strongly alter the
 289 average shape and orientation of γ -ray shower images in the camera. Even
 290 though the orientation of shower images and the image parameter ALPHA
 291 are correlated it is important to investigate the influence of the GF on the
 292 image parameter providing the most powerful discrimination between γ -rays
 293 from a point-like source and unwanted isotropic background (mainly hadrons).



(a) IP = 40 m.



(b) IP = 120 m.

Fig. 8. Normalised distributions of the image parameter ALPHA for 50 GeV γ -rays, $ZA = 0^\circ$, $Az = 0^\circ$ ($\theta = 52^\circ$), 40 m (a) and 120 m impact parameter (b). Different configurations are compared: the distributions indicated by solid lines correspond to $\varphi = 90^\circ$ and 270° , the dash-dotted distributions to $\varphi = 0^\circ$ and 180° , and the distributions indicated by dashed lines to intermediate telescope positions $\varphi = 30^\circ$, 60° , 120° , 150° , 210° , 240° , 300° and 330° . The corresponding distribution obtained without GF in the MC simulation is also plotted (dotted line). The percentage of events with $|\text{ALPHA}| \leq 9^\circ$ is given in the legend.

Figures 8-10 show the ALPHA distributions (normalised to the number of entries) for γ -ray energies of 50 GeV, 450 GeV and 1 TeV. Showers recorded at 40 m and 120 m impact parameter were considered together with the different possible configurations: the distributions indicated by dash-dotted lines correspond to $\varphi = 0^\circ$ and 180° (as defined in figure 2 (a)), where the connecting line between the shower axis and the telescope optical axis is parallel to the north-south direction. This configuration corresponds to shower images which are oriented parallel to the direction of the GF in the camera. The distributions indicated by solid lines were obtained for $\varphi = 90^\circ$ and 270° , where the connecting line between the shower axis and the telescope optical axis is parallel to the east-west direction. In this case the shower images are on average not rotated and oriented normal to the direction of the GF in the camera. The ALPHA distributions indicated by dashed lines belong to intermediate telescope positions $\varphi = 30^\circ$, 60° , 120° , 150° , 210° , 240° , 300° and 330° . The corresponding ALPHA distributions obtained without GF in the MC simulation are also plotted (dotted lines). The percentage of events with $|\text{ALPHA}| \leq 9^\circ$ is given in the legend. The cut is indicated by the vertical dotted line.

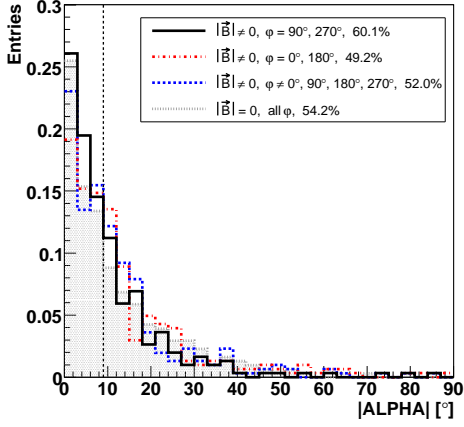
It can be seen that for configurations where the connecting line between the telescope and the shower axis is parallel to the north-south direction (parallel to the direction of the GF) the corresponding ALPHA distributions (red histograms) can be significantly broadened although the corresponding shower

images are on average not rotated. However, the ALPHA distribution for the opposite configuration (connecting line between the telescope and the shower axis parallel to the east-west direction) are stronger peaked at low values due to the influence of the GF (compare figure 9 (a) and (b)). The remaining configurations always lead to broadened ALPHA distributions due to the rotation of the shower images with a preferential direction.

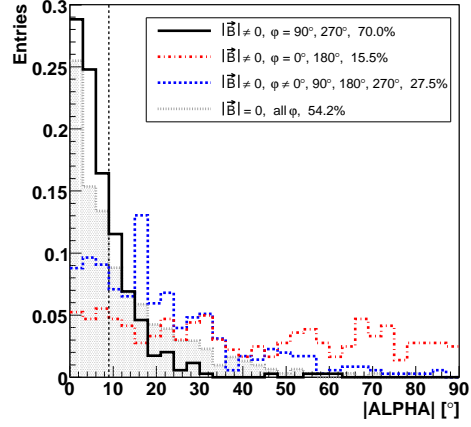
In conclusion it can be stated that the influence of the GF can significantly degrade the orientation discrimination of shower images. It is evident that for some configurations discussed above the γ -ray signal cannot be recovered by de-rotating the shower images.

Figure 11 shows the ALPHA distributions for 450 GeV γ -rays, $ZA = 40^\circ$, $Az = 180^\circ$ and 40 m as well as 120 m impact parameter. The ALPHA distributions obtained without GF (dotted line) are shown together with the distributions obtained for enabled GF (dashed line) and the ones obtained after de-rotation of the shower images (solid line). It is possible to correct for GF effects by de-rotating the shower images. However, if all telescope positions are taken into account ($\varphi = 0^\circ \dots 330^\circ$) the improvement in terms of the percentage of events with $|\text{ALPHA}| \leq 9^\circ$ is less than 8 % (figure 11 (a) and (b)). Ignoring the most unfavourable configurations with respect to the influence of the GF ($\varphi \neq 0^\circ$ and 180°) results in ALPHA distributions which are stronger peaked at small values (figure 11 (c) and (d)). As expected, for the most unfavourable configurations ($\varphi = 0^\circ$ and 180°) the γ -ray signal cannot be recovered by de-rotation. The corresponding images are not rotated but their angular distribution is broadened (figure 11 (e) and (f)).

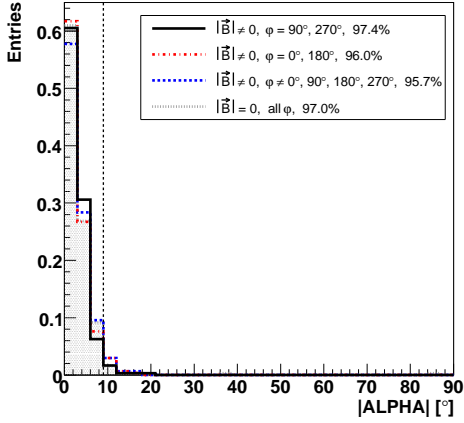
Given that the energy, the rotation angle and the impact parameter is well known in MC, the amount of recovered real γ -ray showers from observational data by de-rotation is expected to be lower. Both the energy and the impact parameter have to be estimated and are thus known less precisely. To be efficient, the de-rotation of the shower images requires a precise knowledge of the impact parameter and the information on the energy of the γ -ray candidates from observational data. Moreover, we focused on intermediate γ -ray energies where the rotation angle is large (figure 5 (d)) and the spread of the ALPHA distribution is rather low. At lower energies than those considered here the recovery of the γ -ray signal is even less efficient [1]. This is also the case for 1 TeV γ -rays, where the ALPHA distribution is stronger peaked at small values and the rotation angle is smaller (figure 5). Because of the relatively poor knowledge of the impact parameter in case of real shower images the improvement in sensitivity by de-rotation of the shower images is expected to be below 10 %.



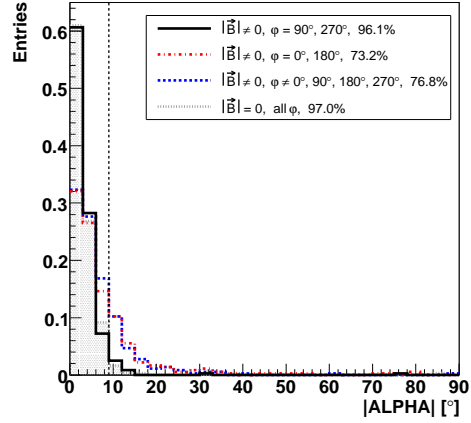
(a) $Az = 0^\circ$, $IP \approx 40$ m, $\theta = 12^\circ$.



(b) $Az = 180^\circ$, $IP \approx 40$ m, $\theta = 87^\circ$.

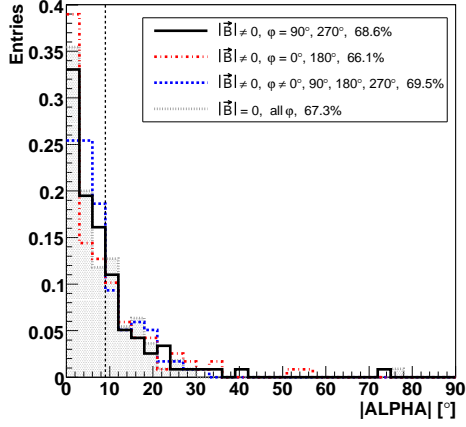


(c) $Az = 0^\circ$, $IP \approx 120$ m, $\theta = 12^\circ$.

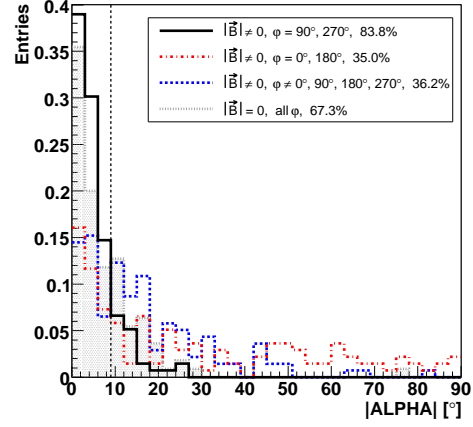


(d) $Az = 180^\circ$, $IP \approx 120$ m, $\theta = 87^\circ$.

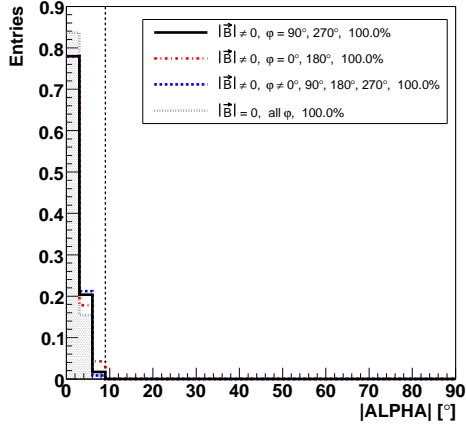
Fig. 9. As figure 8, but for 450 GeV γ -rays, $ZA = 40^\circ$, $Az = 0^\circ$ and 180° .



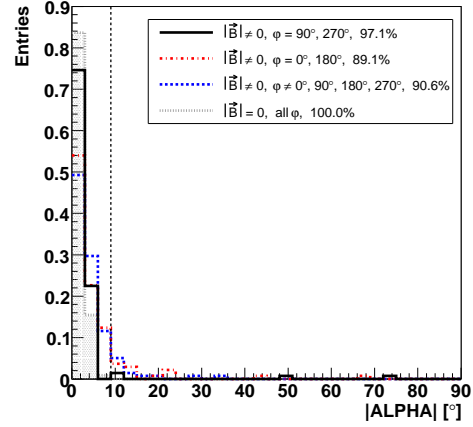
(a) $Az = 0^\circ$, $IP \approx 40$ m, $\theta = 12^\circ$.



(b) $Az = 180^\circ$, $IP \approx 40$ m, $\theta = 87^\circ$.

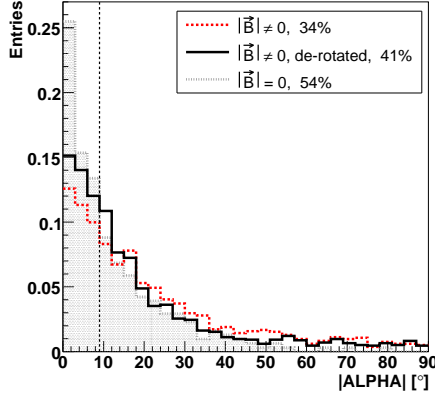


(c) $Az = 0^\circ$, $IP \approx 120$ m, $\theta = 12^\circ$.

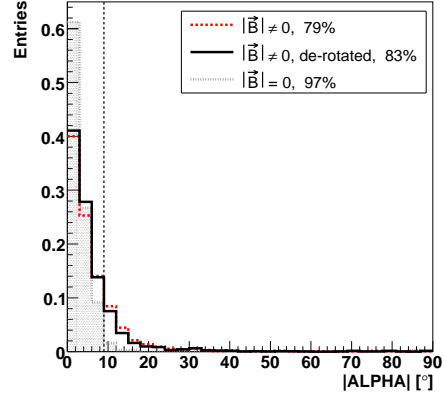


(d) $Az = 180^\circ$, $IP \approx 120$ m, $\theta = 87^\circ$.

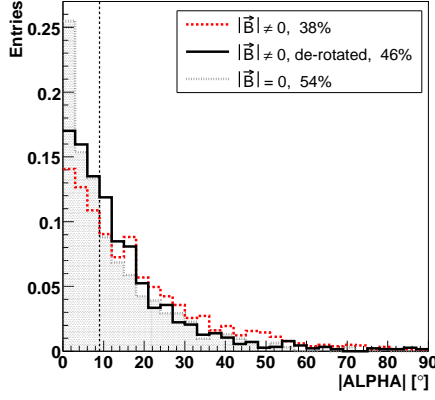
Fig. 10. As figure 8, but for 1 TeV γ -rays, $ZA = 40^\circ$, $Az = 0^\circ$ and 180° .



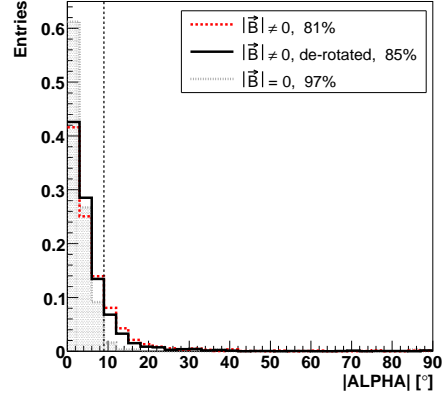
(a) $IP \approx 40 \text{ m}$, $\varphi = 0^\circ \dots 330^\circ$.



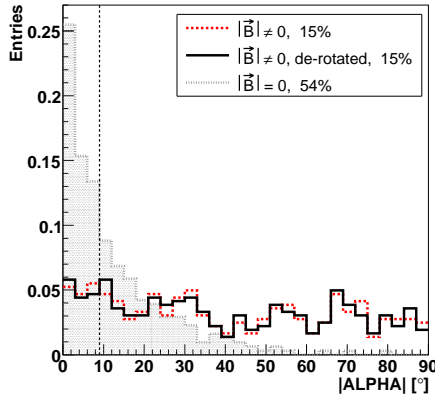
(b) $IP \approx 120 \text{ m}$, $\varphi = 0^\circ \dots 330^\circ$.



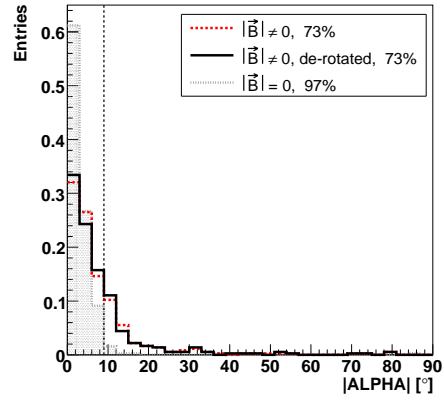
(c) $IP \approx 40 \text{ m}$, $\varphi \neq 0^\circ \text{ and } 180^\circ$.



(d) $IP \approx 120 \text{ m}$, $\varphi \neq 0^\circ \text{ and } 180^\circ$.



(e) $IP \approx 40 \text{ m}$, $\varphi = 0^\circ \text{ and } 180^\circ$.



(f) $IP \approx 120 \text{ m}$, $\varphi = 0^\circ \text{ and } 180^\circ$.

Fig. 11. Normalised distributions of the image parameter ALPHA for 450 GeV γ -rays, $ZA = 40^\circ$ and $Az = 180^\circ$, 40 m ((a), (c) and (e)) and 120 m impact parameter ((b), (d) and (f)). The distributions indicated by dotted lines were obtained without GF and the ones indicated by dashed lines for enabled GF in the MC simulation. For the distributions indicated by solid lines the shower images were de-rotated (see text for more details).

6.3 GF Effects on the DISP-reconstructed γ -ray Arrival Direction

A DISP analysis of the MC γ -ray shower images was performed to study the GF effects on the reconstructed arrival directions.

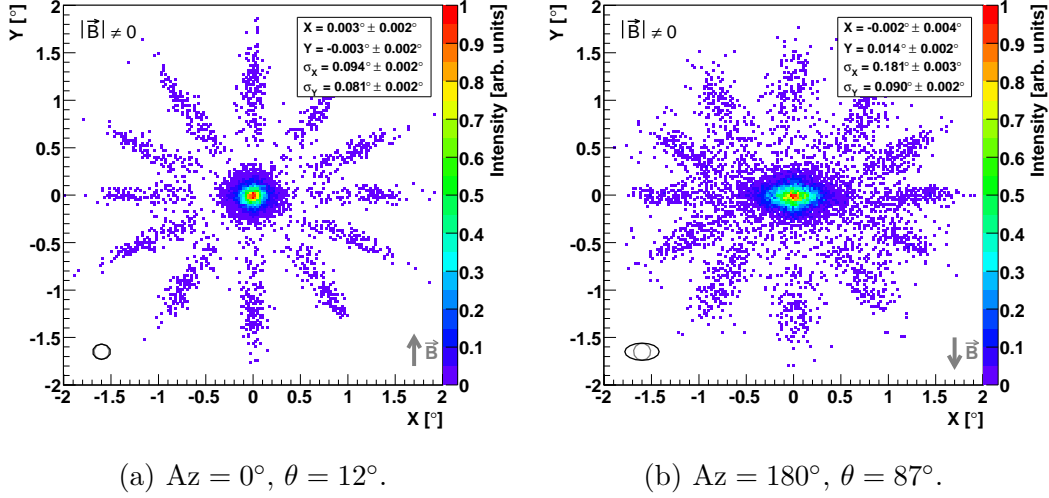
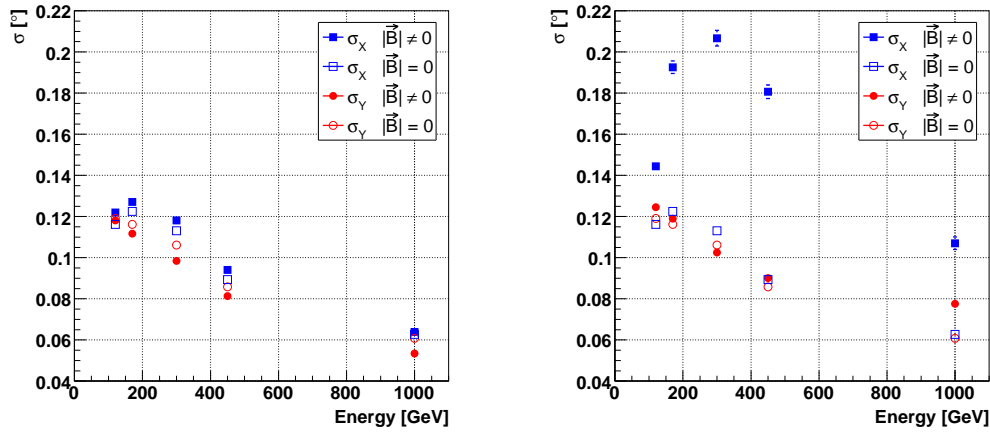


Fig. 12. DISP-reconstructed arrival directions for 450 GeV γ -rays, impact parameters between 60 m and 140 m, $ZA = 40^\circ$, $Az = 0^\circ$ and 180° , respectively (see text for more details).

For the optimisation of the second-order polynomials in equation (1), dedicated MC γ -ray samples with continuous impact parameter distribution between 0 m and 500 m were produced. The MC samples were produced for the same γ -ray energies, ZAs and image cleaning levels as the MC data used for the preceding studies. The EAS core location was randomly placed somewhere in a circle on the plane perpendicular to the direction of the EAS. Also, the MC samples were produced without GF, thus only for $Az = 0^\circ$. In this way the results from the DISP method obtained for different telescope pointing directions are comparable since the DISP polynomials themselves are not subject to GF effects.

Figure 12 shows the DISP-reconstructed arrival directions for 450 GeV γ -rays, impact parameters between 60 m and 140 m, $ZA = 40^\circ$, $Az = 0^\circ$ and 180° . The projected direction of the GF is indicated in the lower right part of the figures, and the ellipticity of the distributions of DISP-reconstructed arrival directions is shown in the lower left part of the figures. The semi-minor and the semi-major axis of the ellipse correspond to the sigma of a Gaussian fit to the distributions using bands of $\Delta_{X,Y} = \pm 0.035^\circ$ parallel and perpendicular to the projected direction of the GF. The size of the bands was arbitrarily chosen, but it is not critical for the result. Within errors, the relative difference of the results obtained from the two orientations is independent of the size of the bands. The result from the Gaussian fit is also shown in the legend. As can be seen from the figures the distributions appear to be significantly

380 elongated perpendicular to the projected direction of the GF, while the peak
 381 of the DISP distribution is always centred at the nominal source position
 382 (camera centre). The extent of the elongation depends on the angle θ between
 383 the shower axis and the direction of the GF. The GF effects on the DISP
 384 method thus result in a degradation of the sky maps in a way that a point-like
 385 γ -ray source appears to be extended, i.e. the γ -ray PSF is degraded. The star-
 386 shaped appearance of the DISP distributions arises from events with wrong
 387 head-tail assignment. The false head-tail assignment cannot be attributed to
 388 GF effects since it occurs also for the favourable telescope pointing direction
 389 (figure 12 (a)). This illustrates the basic limitation of a single telescope to
 390 properly reconstruct the true source position. In case of a single telescope the
 391 DISP method has to rely on the shower asymmetry along the major axis of
 392 the shower image (see section 5).



(a) $Az = 0^\circ$, $ZA = 40^\circ$, $\theta = 12^\circ$.

(b) $Az = 180^\circ$, $ZA = 40^\circ$, $\theta = 87^\circ$.

Fig. 13. Lateral and longitudinal spread of the DISP distribution versus γ -ray energy
 for impact parameters between 60 m and 140 m, $ZA = 40^\circ$, $Az = 0^\circ$ and 180° ,
 respectively (see text for more details).

393 Figure 13 shows the lateral and longitudinal spread versus γ -ray energy for
 394 different orientations of the telescope. The spread is defined as the sigma
 395 of a Gaussian fit to the DISP distribution using bands of $\Delta_{X,Y} = \pm 0.035^\circ$
 396 parallel and normal to the projected direction of the GF in the camera. Impact
 397 parameters between 60 m and 140 m were considered. The figures clearly show
 398 that, compared to the case of disabled GF, the spread of the DISP distribution
 399 increases significantly for an unfavourable telescope orientation (large angle
 400 θ). The maximum spread occurs always perpendicular to the direction of the
 401 GF in the camera. Therefore, depending on the orientation of an EAS with
 402 respect to the telescope and the impact parameter, the DISP-reconstructed
 403 incoming direction of the corresponding primary γ -ray has a large uncertainty.

6.4 GF Effects on the Energy Reconstruction of γ -ray Images

It was previously discussed that the influence of the GF on the shower development affects also the energy reconstruction and the trigger efficiency for γ -rays.

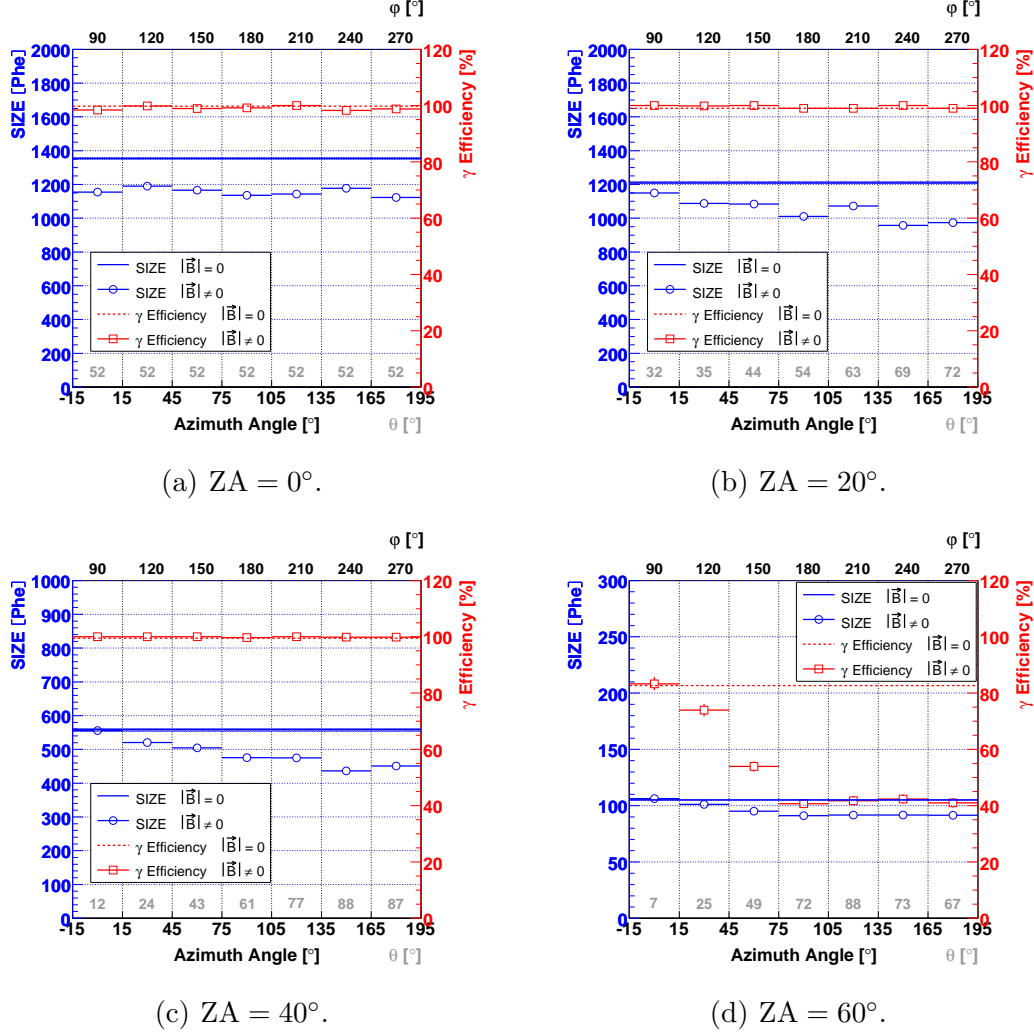


Fig. 14. The mean of the image parameter SIZE and the γ efficiency versus Az angle for 450 GeV γ -rays and ZA between 0° and 60° . The telescope is always situated at angles $\varphi = \text{Az} + 90^\circ$ and 120 m impact parameter.

The east-west separation of electrons and positrons in EAS due to the GF modifies the Cherenkov distribution on the ground such that the reconstructed Cherenkov light, i.e. the integrated light content of the shower images is reduced for unfavourable shower orientations with respect to the direction of the GF.

Figure 14 shows the average reconstructed light content of shower images together with the γ efficiency versus Az angle for 450 GeV energy γ -rays and

415 ZAs between 0° and 180° . To compare equivalent configurations (see figure 2
 416 (a)) the telescope is always situated at angles $\varphi = Az + 90^\circ$ and the impact
 417 parameter was set to 120 m. The angle θ between the direction of the EAS and
 418 the GF is given on top of the abscissa. The γ efficiency is defined as the ratio
 419 of the number of γ -ray showers surviving the trigger and the image cleaning
 420 to the number of generated γ -rays. From figure 14 (d) it can be seen that the
 421 γ efficiency varies by up to 50 %. For showers close to the trigger threshold
 422 the Cherenkov light distribution on the ground can be thinned out such that
 423 most of the events do not survive the trigger level. This occurs only for show-
 424 ers close to the energy threshold of the telescope, which is ZA dependent.
 425 For some telescope pointing directions the total reconstructed integrated light
 426 of shower images can be reduced by up to ~ 20 %. This is not only the case for
 427 low energies but also for TeV γ -rays. Consequently, if GF effects are not taken
 428 into account the energy of γ -ray candidates from observational data will be
 429 systematically underestimated whereas the γ efficiency will be overestimated.
 430 Both effects degrade the determination of the flux from a γ -ray source if they
 431 are not properly taken into account in the MC simulation.

432 7 Conclusions

433 The results from the MC studies show that the GF can significantly affect
 434 both the shape and the orientation of shower images recorded with an IACT
 435 like MAGIC. Therefore, the orientation discrimination of γ -rays against un-
 436 wanted (hadronic) background can be significantly degraded. It was demon-
 437 strated that the de-rotation of the shower images does not help to recover the
 438 pointing entirely. At most 10 % of the events can be recovered by de-rotation
 439 requiring the knowledge of the impact parameter and energy of the γ -rays.
 440 The influence of the GF also degrades the DISP-estimated arrival direction
 441 of MC-generated γ -rays. Due to the influence of the GF on the development
 442 of EAS the DISP distribution can be significantly elongated perpendicular to
 443 the projection of the GF in the camera. The quality of a sky map is degraded
 444 in a way that a point-like source appears extended unless it is compared to
 445 a proper MC simulation taking into account the trajectory of the source in
 446 the sky. However, the peak of the DISP distribution is always centred at the
 447 source position.
 448 It was also shown that the influence of the GF on EAS can significantly affect
 449 the energy reconstruction and the trigger efficiency for γ -rays. If this effect is
 450 not taken into account, the energy of γ -ray candidates from observational data
 451 will be systematically underestimated (up to ~ 20 % effect). For low energies
 452 close to the analysis threshold (< 100 GeV) the γ efficiency also depends on
 453 the position of the telescope in the Cherenkov light pool [1]. At higher energies
 454 (~ 300 GeV - 1 TeV), the γ efficiency is affected only at large ZA, where the

455 telescope threshold energy is significantly increased ($\lesssim 50\%$ effect).
 456 It was demonstrated that the extent of the GF effects not only depends on
 457 the orientation of EAS with respect to the direction of the GF but also on
 458 the position of the telescope with respect to the EAS core location on ground.
 459 Shower images are not only rotated away from the projected direction of the
 460 GF in the telescope camera plane but can also be rotated towards it, contrary
 461 to what was reported in [8].
 462 Altogether, GF effects on EAS affect the γ -ray sensitivity of an IACT and the
 463 determination of the flux from a VHE γ -ray source. Distinct MC data covering
 464 the same ZA and Az angle range as the observational data being analysed are
 465 required to account for GF effects.
 466 It is remarkable that the GF effects not only occur at very low energies but also
 467 at high energies around 1 TeV. The GF effects are rather pronounced at γ -ray
 468 energies around 450 GeV. The reason for GF effects to occur at high energies
 469 is presumably linked to a characteristic feature in the development of a γ -ray
 470 induced EAS. The process of multiplication in EAS continues until the aver-
 471 age energy of the shower particles is insufficient to further produce secondary
 472 particles in subsequent collisions. At this stage of the shower development,
 473 the shower maximum is reached (largest number of secondary particles) and
 474 the average energy of the secondaries is close to the so-called critical energy
 475 of ~ 100 MeV [26] below which secondary electrons and positrons lose their
 476 energy predominantly through ionisation of air molecules [27]. At the shower
 477 maximum, the average energy of the secondary particles is independent of the
 478 primary γ -ray energy and the GF has on average the same influence on the
 479 secondary particles.
 480 Apart from that, the average atmospheric depth at which the shower maximum
 481 occurs increases logarithmically with increasing energy of the primary γ -ray
 482 [27], and therefore the track along which secondary electrons and positrons
 483 suffer from Lorentz deflection increases, too.
 484 Another point worthy of mentioning is the fact that the threshold energy for
 485 a charged particle to emit Cherenkov light decreases with increasing atmo-
 486 spheric depth. Hence, in high-energy EAS, even charged secondaries of lower
 487 energy suffering strong Lorentz deflection may additionally contribute to the
 488 Cherenkov light pool on ground.
 489 GF effects on the hadron induced background were not studied. It is impos-
 490 sible to show the rotation effect using shower images from hadron candidates
 491 of observational data, because they do not point to any source. Also, possible
 492 GF effects on the hadron induced background presumably do not degrade the
 493 background discrimination. Close to the energy threshold the trigger efficiency
 494 for the hadronic background should be reduced, too.

496 Although this study focuses on GF effects relevant for a single IACT like
 497 MAGIC the influence of the GF on the development of EAS is expected to de-
 498 grade also the performance of stereoscopic IACT arrays. In a stereoscopic tele-
 499 scope system multiple telescopes view the same EAS. The individual images
 500 are then combined to form a common event. Therefore, stereoscopic systems
 501 allow for a three-dimensional reconstruction of the shower axis resulting in an
 502 improved sensitivity. The shower direction on the sky is estimated from the
 503 intersection point of the major image axes in a composite field of view, on an
 504 event by event basis [22]. Due to the rotation of the individual shower images
 505 the intersection point will be modified in a way that the source direction in
 506 the sky is wrongly reconstructed. Stereoscopic systems do not trigger homoge-
 507 neously but preferably on EAS with impact positions between the telescopes.
 508 As the impact distance on ground between the EAS and the individual tele-
 509 scopes of an array is different in the majority of cases, the GF will deteriorate
 510 the orientation of the individual shower images differently. As a result the per-
 511 formance of stereoscopic IACT arrays is degraded by GF effects. A detailed
 512 MC study on the influence of GF effects on the performance of stereoscopic
 513 IACT systems is in preparation.

514 The intensity of the GF on the Earth' surface ranges from about $20 \mu\text{T}$ to
 515 about $70 \mu\text{T}$ [17]. It is therefore important to take into account the GF effects
 516 for the site selection of future projects utilising the imaging air Cherenkov
 517 technique. To minimise the influence of the GF on the detector performance
 518 it is mandatory to select a site with a low absolute value of the GF. Hence, the
 519 best-suited location would be close to the so-called South Atlantic Anomaly,
 520 where the GF strength is minimal, amounting to about one half of the value
 521 for the MAGIC telescope site.

522 It is difficult to study GF effects in observational data. The elevation effect on
 523 shower images complicates such studies. Directions with strong magnetic field
 524 correspond to large ZA and the sensitivity of an IACT changes as a function of
 525 the ZA as a result of changing shower image characteristics due to increasing
 526 air mass with increasing ZA [22]. There are several requirements a γ -ray source
 527 should fulfil to be an appropriate candidate for GF studies in observational
 528 data: it should be strong, preferably point-like, stable and it should follow a
 529 trajectory corresponding to a large GF component normal to the telescope
 530 pointing direction (figure 1 (a)).

531 Preliminary results from studies on GF effects in observational data taken with
 532 MAGIC were already shown in [1,28]. It was demonstrated that the pointing
 533 resolution of MAGIC allows to study GF effects in observational data even for
 534 a very low component of the GF normal to the shower direction. However, an
 535 extensive study on GF effects in observational data is in progress.

536 References

- 537 [1] S.C. Commichau, Observation of Very High Energy Gamma-Rays from the
538 Galactic Center with the MAGIC Telescope considering Geomagnetic Field
539 Effects on the Imaging Technique, Ph.D. Thesis (No. 17118), ETH Zürich, 2007.
- 540 [2] A. Wenger, Diploma Thesis, The effect of the earth's magnetic field on extensive
541 air showers, ETH Zürich, 2004.
- 542 [3] R. de los Reyes-Lopez R, Ph.D. Thesis, UC Madrid, 2008.
- 543 [4] G. Cocconi, Influence of the Earth's Magnetic Field on the Extensive Air
544 Showers, Physical Review 93 (1954) 646.
- 545 [5] N.A. Porter, Nuovo Cimento Lett. 8 (1973) 481.
- 546 [6] C.C.G. Bowden et al., The effect of the geomagnetic field on TeV γ -ray
547 detection, J. Phys. G: Nucl. Part. Phys. 18 (1992) L55.
- 548 [7] M.J. Lang et al., A search for geomagnetic effect on the sensitivity of the
549 atmospheric Cherenkov imaging technique, J. Phys. G: Nucl. Part. Phys. 20
550 (1994) 1841.
- 551 [8] P.M. Chadwick et al., Geomagnetic effects on atmospheric Čerenkov images, J.
552 Phys. G: Nucl. Part. Phys. 25 (1999) 1223.
- 553 [9] P.M. Chadwick, Geomagnetic Effects on the Performance of Atmospheric
554 Čerenkov Telescopes, Proc. 26th Int. Cosmic Ray Conf. 5 (1999) 231.
- 555 [10] P.M. Chadwick et al., The correction of atmospheric Čerenkov images for the
556 effect of the geomagnetic field, J. Phys. G: Nucl. Part. Phys. 26 (2000) L5.
- 557 [11] K.M. Aye et al., Correcting high resolution imaging for the effects of the
558 geomagnetic field, Proc. 27th Int. Cosmic Ray Conf. 7 (2001) 2842.
- 559 [12] E. Lorenz, Status of the 17 m \varnothing MAGIC telescope, New Astr. Rev. 48 (2004)
560 339.
- 561 [13] J.A. Barrio et al., The MAGIC telescope design report, MPI Institute Report
562 MPI-PhE/98-5, Munich, 1998.
- 563 [14] F. Goebel et al. (MAGIC Collab.), Status of the second phase of the MAGIC
564 telescope, Proc. 30th Int. Cosmic Ray Conf., Merida, 2007.
- 565 [15] J. Albert et al. (MAGIC Collab.), VHE γ -Ray Observation of the Crab Nebula
566 and its Pulsar with the MAGIC Telescope, Astrophys. J. 674 (2008) 1037.
- 567 [16] D. Heck et al., Report FZKA 6019 (1998), Forschungszentrum Karlsruhe;
568 <http://www-ik.fzk.de/corsika/>
- 569 [17] National Geographic Data Center (NGDC);
570 <http://www.ngdc.noaa.gov/geomag/>

- 571 [18] P. Majumdar et al. (MAGIC Collab.), Monte Carlo simulation for the MAGIC
572 telescope, Proc. 29th Int. Cosmic Ray Conf. 5 (2005) 203.
- 573 [19] A.M. Hillas, Cherenkov light images of EAS produced by primary gamma rays
574 and by nuclei, Proc. 19th Int. Cosmic Ray Conf. 3 (1985) 445.
- 575 [20] T. Bretz and R.M. Wagner (MAGIC Collab.), The MAGIC Analysis and
576 Reconstruction Software, Proc. 28th Int. Cosmic Ray Conf. 5 (2003) 2947.
- 577 [21] R. Mirzoyan and E. Lorenz, Measurement of the night sky light background at
578 La Palma, MPI Institute Report MPI-PhE/94-35, Munich, 1994.
- 579 [22] D.J. Fegan, γ /hadron separation at TeV energies, J. Phys. G: Nucl. Part. Phys.
580 23 (1997) 1013.
- 581 [23] V.P. Fomin et al., New methods of atmospheric Cherenkov imaging for gamma-
582 ray astronomy. I. The false source method, Astropart. Phys. 2 (1994) 137.
- 583 [24] R.W. Lessard et al., A new analysis method for reconstructing the arrival
584 direction of TeV gamma rays using a single imaging atmospheric Cherenkov
585 telescope, Astropart. Phys. 15 (2001) 1.
- 586 [25] E. Domingo-Santamaría et al. (MAGIC Collab.), The DISP analysis method
587 for point-like or extended γ source searches/studies with the MAGIC Telescope,
588 Proc. 29th Int. Cosmic Ray Conf. 5 (2005) 363.
- 589 [26] H. Bethe and W. Heitler, On the Stopping of Fast Particles and on the Creation
590 of Positive Electrons, Proc. R. Soc. 146 (1934) 83.
- 591 [27] K. Greisen, Progress in Cosmic Ray Physics 3 (1956) 27.
- 592 [28] S.C. Commichau et al. (MAGIC Collab.), Geomagnetic Field Effects on the
593 Imaging Air Shower Cherenkov Technique, Proc. 30th Int. Cosmic Ray Conf.,
594 Merida, 2007.